Local Energetic Constraints on Walker Circulation Strength

ROBERT C. WILLS

ETH Zürich, Zurich, Switzerland, and California Institute of Technology, Pasadena, California

XAVIER J. LEVINE

Yale University, New Haven, Connecticut

TAPIO SCHNEIDER

ETH Zürich, Zurich, Switzerland, and California Institute of Technology, Pasadena, California

(Manuscript received 25 July 2016, in final form 20 January 2017)

ABSTRACT

The weakening of tropical overturning circulations is a robust response to global warming in climate models and observations. However, there remain open questions on the causes of this change and the extent to which this weakening affects individual circulation features such as the Walker circulation. The study presents idealized GCM simulations of a Walker circulation forced by prescribed ocean heat flux convergence in a slab ocean, where the longwave opacity of the atmosphere is varied to simulate a wide range of climates. The weakening of the Walker circulation with warming results from an increase in gross moist stability (GMS), a measure of the tropospheric moist static energy (MSE) stratification, which provides an effective static stability for tropical circulations. Baroclinic mode theory is used to determine changes in GMS in terms of the tropical-mean profiles of temperature and MSE. The GMS increases with warming, owing primarily to the rise in tropopause height, decreasing the sensitivity of the Walker circulation to zonally anomalous net energy input. In the absence of large changes in net energy input, this results in a rapid weakening of the Walker circulation with global warming.

1. Introduction

In climate models and observations, convective mass flux and zonally anomalous tropical overturning circulations, such as the Walker circulation, weaken robustly in response to global warming (Vecchi et al. 2006; Vecchi and Soden 2007; Merlis and Schneider 2011). Associated with this weakening is a reduction of tropical precipitation contrasts (Wills and Schneider 2016; Wills et al. 2016) and a modification of extratropical Rossby waves, which influence midlatitude temperature and precipitation patterns (Seager et al. 2005). A quantitative theory for the strength of convective mass fluxes and zonally anomalous tropical overturning circulations is needed to constrain the associated impacts on tropical precipitation and midlatitude teleconnections.

Global energetic constraints on evaporation and precipitation lead to a reduction of the strength of convective mass fluxes globally in response to increasing near-surface specific humidity with global warming (Betts 1998; Held and Soden 2006; Vecchi and Soden 2007; Schneider et al. 2010). This results in a weakening of zonally anomalous tropical circulations, in which the bulk of the global convective mass fluxes occur (Held and Soden 2006; Vecchi and Soden 2007). Zonal-mean circulations such as the Hadley circulation have to obey additional constraints—for example, from the angular momentum balance (Held and Hou 1980; Walker and Schneider 2006; Schneider 2006)—and therefore are less free to respond to energetic changes alone than the zonally anomalous circulations. However, even for zonally anomalous circulations, the global energetic constraints do not provide a quantitative theory for local circulation changes.

Merlis and Schneider (2011) use the atmospheric moisture budget to construct a local theory for the strength of zonally anomalous tropical circulations forced by zonally anomalous ocean heat flux convergence. This

Corresponding author: Robert C. Wills, rcwills@uw.edu

DOI: 10.1175/JAS-D-16-0219.1

theory explains the weakening of the Walker circulation in terms of the rapid increase in atmospheric moisture content and moisture stratification with global warming. However, it requires knowledge of changes in precipitation anomalies in the ascending branch of the Walker circulation, which are small compared to changes in atmospheric moisture content in their idealized general circulation model (GCM) simulations. Precipitation changes are small as a consequence of small changes in zonally anomalous evaporation, which is constrained energetically by the prescribed ocean heat flux convergence, and small changes in zonally anomalous precipitation minus evaporation ($P - E$), which results from a cancellation between thermodynamic and dynamic changes in the moisture budget with warming. This cancellation is also seen in comprehensive climate models (Seager et al. 2010; Chadwick et al. 2013; Wills et al. 2016) but is a direct consequence of the reduction in circulation strength, thus making this a circular argument. The atmospheric moisture budget provides a useful link between changes in circulation and changes in precipitation, but it does not provide a way of knowing one without assuming the other.

Knutson and Manabe (1995) analyze the local energetic balances in the ascending and descending regions of the Walker circulation. Under a quadrupling of atmospheric CO_2, they find that the increased latent heating in the ascending branch of the Walker circulation is balanced primarily by an increase in dry static stability, which increases the dynamic cooling by vertical motions. This helps rule out the need for an increased Walker circulation strength to balance the increased latent heating through enhanced adiabatic cooling. It does not, however, provide a quantitative theory for Walker circulation strength, as both the latent heating and adiabatic cooling are coupled to vertical motion.

A number of studies have used the moist static energy (MSE) budget and baroclinic mode theory to remove this cancellation between latent heating and adiabatic cooling and further constrain tropical circulations (Neelin and Held 1987; Neelin and Zeng 2000; Chou and Neelin 2004; Chou et al. 2009; Chou and Chen 2010). In particular, Chou and Neelin (2004) propose a mechanism according to which the strength of tropical overturning circulations is reduced with warming because of an increase in gross moist stability (GMS), the effective static stability felt by tropical circulations. The increase in GMS is due to an increasing depth of deep convection and is partially cancelled by an increase in lower-tropospheric specific humidity (Chou and Chen 2010; Chou et al. 2013). These changes increase the energy required to maintain the time-mean Walker circulation. This is closely related to the warm-gets-wetter mechanism, according to which ocean regions with enhanced surface warming relative to the tropical mean experience locally reduced GMS and enhanced precipitation (Xie et al. 2010; Huang et al. 2013). In this paper, we investigate how GMS constrains changes in the Walker circulation strength across a wide range of climates in an idealized GCM.

In the real climate system, the Walker circulation is coupled to interannual variability of tropical Pacific SST as part of El Niño–Southern Oscillation (ENSO) (Philander 1990). Additionally, cloud and water vapor radiative effects in convective regions result in leading-order modifications of the net energy input to the atmosphere (Ramanathan et al. 1989; Hartmann et al. 2001). These factors complicate an analysis of modeled changes in the atmospheric energy budget with warming in regions of tropical deep convection. Here, we examine the response of a Walker circulation forced by prescribed tropical ocean heat flux convergence to global warming across a wide range of climates in an idealized GCM without water vapor or cloud radiative effects. The simplicity of our model is an advantage, because the net energy input to the atmosphere is determined almost entirely by the external forcing, allowing a simple assessment of the factors controlling the sensitivity to this forcing.

We construct a theory for changes in GMS that constrains the strength of the Walker circulation in terms of the net energy input. As a result, the Walker circulation strength can be determined from tropical-mean profiles of temperature and MSE and the zonally anomalous net energy input in the ascending branch. The zonally anomalous net energy input, which is determined by prescribed ocean heat fluxes in our experiments, can easily be generalized to real-world situations with time-variable ocean heat fluxes and radiative feedbacks.

We describe the idealized GCM experiments in section 2. In section 3, we analyze the MSE budget and use the dominant balance to diagnose changes in Walker circulation strength based on the GMS. We also introduce a quasi-equilibrium theory for the GMS, which relates GMS to the tropical-mean temperature and MSE profiles. In section 4, we relate changes in the warm pool $P - E$ anomaly to changes in Walker circulation strength. We provide discussion of the connection of this work to work on tropical SST contrasts and cloud feedbacks in section 5. In section 6, we present our conclusions.

2. Idealized GCM experiments

To study the response of the tropical atmosphere to prescribed ocean heat fluxes, we use the idealized moist

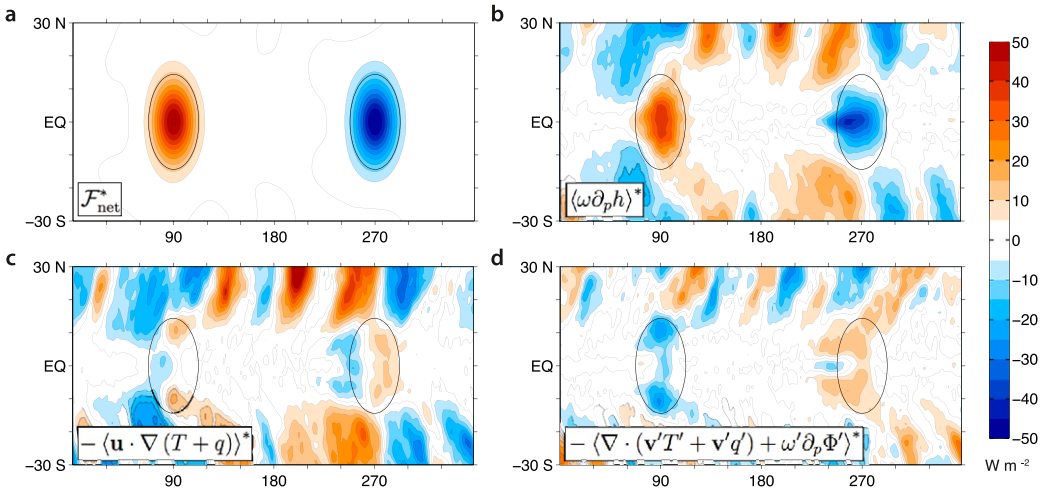

FIG. 1. Zonally anomalous MSE budget [Eq. (4)] in the reference climate, integrated from the surface to the tropopause (plots are indistinguishable if the integration is continued to the top of the atmosphere). (a) Zonally anomalous net energy input $\mathcal{F}^*_{\rm net}$. (b) Vertical MSE advection $\langle\omega\partial_p h\rangle^*$. (c) Horizontal MSE advection $-\langle\mathbf{u}\cdot\nabla(T+q)\rangle^*$. (d) Transient-eddy MSE advection $-\langle\nabla\cdot(\mathbf{v}'T'+\mathbf{v}'q')+\omega'\partial_p\Phi'\rangle^*$. Signs are chosen such that all other terms add up to the vertical motion term $\langle\omega\partial_p h\rangle^*$. Black contours show where the imposed surface heating $\mathcal{Q}^*$ is above 10 W m^{-2} or below −10 W m^{-2}. The transient-eddy term is computed as a residual.

GCM of O'Gorman and Schneider (2008), which is based on that of Frierson et al. (2006) and uses the GFDL spectral dynamical core. A quasi-equilibrium convection scheme is used to parameterize moist convection (Frierson 2007). We prescribe a perpetual-insolation profile resembling Earth's annual-mean profile, as in O'Gorman and Schneider (2008). The atmosphere absorbs broadband longwave fluxes but lacks interactive water vapor and cloud radiative effects.

We force a Walker circulation by prescribing a zonally anomalous ocean heat flux divergence (Q flux) using a slab-ocean aquaplanet boundary condition with 1-m mixed-layer depth. These simulations are described in further detail in Wills and Schneider (2016). The zonally anomalous Q flux is constrained to the equatorial regions and has the form

$$\mathcal{Q}^*(\lambda,\phi) = Q_1 \exp\left[-\frac{(\lambda-\lambda_E)^2}{2\sigma_\lambda^2}-\frac{\phi^2}{2\sigma_\phi^2}\right] - Q_1 \exp\left[-\frac{(\lambda-\lambda_W)^2}{2\sigma_\lambda^2}-\frac{\phi^2}{2\sigma_\phi^2}\right], \quad (1)$$

where $Q_1 = 50\,\mathrm{W\,m^{-2}}$, $\lambda_W = 90°$, $\lambda_E = 270°$, $\sigma_\lambda = 12.5°$, and $\sigma_\phi = 8°$, as in Wills and Schneider (2016). Our simulations differ from those in Merlis and Schneider (2011) only by small differences in the aspect ratio (zonal vs meridional elongation) and amplitude of the Q fluxes. They were chosen as a representative example from the suite of simulations in Wills (2016).

This zonally asymmetric Q flux integrates to zero in the zonal mean, such that its effect on the zonal-mean circulation (i.e., Hadley cells) is negligible. We prescribe a zonal-mean Q flux, representing ocean heat transport from the equatorial region to the subtropics, as in Bordoni and Schneider (2008), such that the Hadley circulation strength and extent in the reference simulation are comparable to that in Earth's annual-mean climate (Levine and Schneider 2011). This helps ensure that the tropical-mean surface temperature and stratification in the reference simulation are close to modern values.

The net zonally anomalous energy input to atmospheric columns, after accounting for zonal anomalies in net radiation, is shown in Fig. 1a. Zonal anomalies in net radiation are small because of the lack of water vapor and cloud radiative effects in our model. In simulations in which we include a water vapor radiative effect using the simple representation of Merlis and Schneider (2010), zonal anomalies in net radiation are still small (not shown), but the water vapor feedback leads to differences in the mean climate (e.g., tropical-mean stratification), which can modify the Walker circulation.

Global warming is simulated by rescaling the reference optical depth, $\tau = \alpha\tau_{\rm ref}$, where $\tau_{\rm ref}$ is a function of latitude and height (O'Gorman and Schneider 2008). We use 14 values of the rescaling parameter α between 0.6 and 6.0 to simulate climates with global-mean surface temperatures ranging from 280 to 316 K. Each simulation is spun up for 4 yr, then averaged over the subsequent 8 yr.

3. A local energetic theory of the Walker circulation strength

a. Zonal asymmetries in the MSE budget

The MSE budget and baroclinic mode theory are often used together to model divergent circulations in the tropics (Neelin and Held 1987; Neelin and Zeng 2000; Chou and Neelin 2004; Neelin 2007). The MSE budget combines the thermodynamic energy and moisture budgets, leading to a cancellation of adiabatic cooling and latent heating. It can be expressed as

$$\partial_t\langle T+q\rangle + \langle \mathbf{u}\cdot\nabla(T+q)\rangle + \langle \omega\partial_p h\rangle = \mathcal{F}_{\text{net}}, \qquad (2)$$

where the angle brackets denote a mass-weighted vertical integral over the troposphere, $\mathcal{F}_{\text{net}}$ is the net energy input to an atmospheric column, $\mathbf{u}$ is the horizontal wind on pressure levels, ω is the vertical pressure velocity, and $h = T + \Phi + q$ is the MSE, determined in terms of temperature T, geopotential Φ, and specific humidity q (temperature and specific humidity have absorbed factors of specific heat capacity and latent heat of vaporization, such that they are in units of joules per kilogram). The net energy input can be combined with the surface energy balance to express it in terms of the net incoming shortwave radiation $\mathcal{S}$ and outgoing longwave radiation $\mathcal{L}$ at the top of the atmosphere, and the energy uptake $\mathcal{Q}$ by the (ocean) surface,

$$\mathcal{F}_{\text{net}} = \mathcal{S} - \mathcal{L} - \mathcal{Q}. \qquad (3)$$

To focus on zonally anomalous circulations, we investigate zonal anomalies in the time-mean MSE budget,

$$\langle \mathbf{u}\cdot\nabla(T+q)\rangle^* + \langle \omega\partial_p h\rangle^* + \langle \nabla\cdot(\mathbf{v}'T' + \mathbf{v}'q') + \omega'\partial_p\Phi'\rangle^* = \mathcal{F}^*_{\text{net}}. \qquad (4)$$

Here, a prime denotes a departure from the time mean and an asterisk denotes a departure from the zonal mean, which is denoted by square brackets. Time averages are omitted from the notation for clarity and are implied on all quantities throughout the rest of the text. The zonally anomalous net energy input is dominated by the ocean heat flux convergence, which influences the atmosphere primarily through evaporative cooling of the surface E (cf. Merlis and Schneider 2011):

$$\mathcal{F}^*_{\text{net}} \approx -\mathcal{Q}^* \approx E^*. \qquad (5)$$

Other contributions to $\mathcal{F}^*_{\text{net}}$ include zonally anomalous longwave radiative tendencies, but they are generally small in the idealized GCM because of the lack of water vapor and cloud radiative tendencies.

The dominant balance in the tropical convective region is the weak temperature and weak moisture gradient balance (Neelin and Held 1987; Sobel et al. 2001) between the zonally anomalous net energy input $\mathcal{F}^*_{\text{net}}$ (Fig. 1a) and the vertical advection of MSE $\langle\omega\partial_p h\rangle^*$ (Fig. 1b):

$$\langle\omega\partial_p h\rangle^* \sim \mathcal{F}^*_{\text{net}}. \qquad (6)$$

The vertical-advection term $\langle\omega\partial_p h\rangle^*$ can be approximated by the contribution from stationary-eddy circulations $\langle\omega^*\partial_p[h]\rangle$, such that

$$\langle\omega^*\partial_p[h]\rangle \sim \mathcal{F}^*_{\text{net}}. \qquad (7)$$

This is a consequence of zonal anomalies in h being small compared to zonal anomalies in ω in our simulations. The stationary- and transient-eddy advection terms (Figs. 1c,d) also play a role, especially on the edges of the convective region, as discussed by Chou and Neelin (2004). They are generally smaller than the vertical advection term because horizontal MSE gradients are small in the deep tropics. In our analysis, the transient-eddy term is computed as a residual.

The dominant balance (7) of the zonally anomalous MSE budget holds across the range of climates simulated in the idealized GCM (Fig. 2). The transient-eddy flux of MSE reduces the energy available to the Walker circulation by about 20% throughout the range of climates, but it changes little with warming. The time-mean flow horizontal advection term is small in all climates but changes significantly with warming, introducing some errors in the Walker circulation scalings that follow.

b. Gross moist stability and Walker circulation strength

The dominant balance (7) of the MSE budget constrains zonally anomalous vertical velocities ω^* in terms of the zonally anomalous net energy input and the MSE stratification. We focus in particular on the upwelling branch of the Walker circulation, by averaging ω^* over the fixed region where the ocean heat flux convergence is greater than $10\,\text{W}\,\text{m}^{-2}$. The vertical velocity profiles in the ascent region (Fig. 3a) peak in the midtroposphere; the height of convective outflow rises with global warming as the tropopause rises (Fig. 3b).

The weakening of the Walker circulation with warming can be characterized by the stationary-eddy vertical velocity at the pressure level where its absolute value is maximum: ω^*_{max} (Fig. 4a). This definition avoids confounding changes in circulation strength with

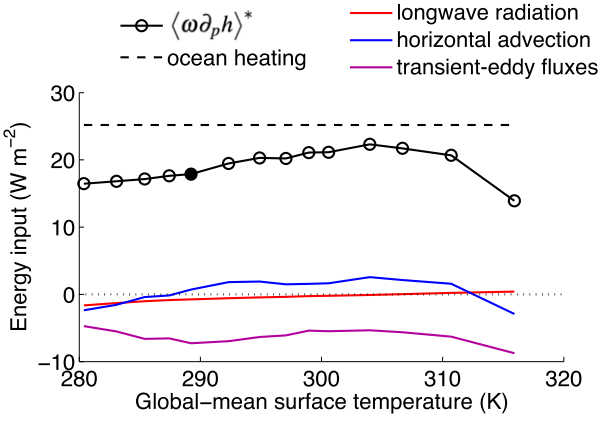

FIG. 2. Changes in zonally anomalous moist static energy budget [Eq. (4)] averaged over the ascent region, across the range of climates simulated. The vertical motion term $\langle\omega\partial_p h\rangle^*$ is primarily balanced by the imposed zonally anomalous ocean heat flux convergence, with some compensation by transient-eddy MSE fluxes. The reference climate (289-K global-mean surface temperature) is indicated with a filled circle. The transient-eddy term is computed as a residual.

changes in the depth of the circulation and is consistent with other studies of zonally anomalous circulations (Merlis and Schneider 2011; Levine and Boos 2016). We define a gross moist stability $\mathcal{M}$, based on the value of $\omega^*_{\max}$ in each simulation, which characterizes the MSE stratification felt by the Walker circulation:

$$\mathcal{M} \equiv -g\frac{\langle\omega^*\partial_p[h]\rangle}{\omega^*_{\max}}. \tag{8}$$

The GMS (J kg^{-1}) increases throughout the range of climates (Fig. 4b), increasing the energy exported out of the convective region per unit convective mass flux. In this framework, the Walker circulation strength is simply determined by the net energy available divided by the gross moist stability,

$$\omega^*_{\max} = -g\frac{\langle\omega^*\partial_p[h]\rangle}{\mathcal{M}}. \tag{9}$$

The large increase in GMS with warming (Fig. 4b) leads to a weakening of the Walker circulation with warming (Fig. 4a), because the energy available for the vertical advection of MSE, $\langle\omega^*\partial_p[h]\rangle$, is constrained by the column energy budget [Eqs. (4)–(7)].

Using the dominant balance (7) of the MSE budget, a scaling can be developed that relates the Walker circulation strength to the net zonally anomalous energy input to an atmospheric column:

$$\omega^*_{\max} \sim -g\frac{\mathcal{F}^*_{\text{net}}}{\mathcal{M}}. \tag{10}$$

Because changes in radiation are small in our model, $\mathcal{F}^*_{\text{net}}$ and thus $\langle\omega^*\partial_p[h]\rangle$ are roughly constant across the range of climates (Fig. 2). In Fig. 4a, we show the strength of the Walker circulation that would result if $\langle\omega^*\partial_p[h]\rangle$ (i.e., approximately the zonally anomalous net energy input) were fixed at its value in the reference climate. This scaling for the Walker circulation strength, which results solely from changes in GMS, captures the weakening of the circulation with warming.

Changes in the zonally anomalous net energy input $\mathcal{F}^*_{\text{net}}$ are expected to be more complex in the real climate system because of cloud and water vapor radiative effects and because of the temporal variation of ocean heat fluxes, for example, with ENSO (Philander 1990). The potential roles of cloud and water vapor radiative effects in the climatological Walker circulation and the Walker circulation response to warming are discussed in section 5. Regardless of the top-of-atmosphere energetic

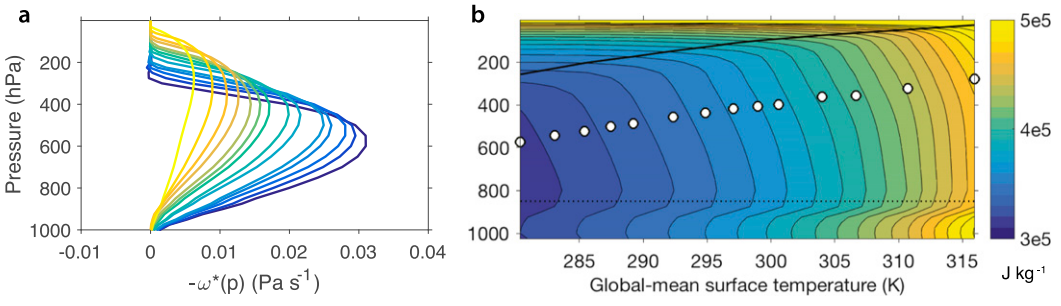

FIG. 3. (a) Stationary-eddy vertical velocity profiles averaged over the ascent region. Profiles are shown for 14 mean climate states color coded from coldest (blue) to warmest (yellow). (b) Vertical profile of zonal-mean moist static energy as a function of global-mean surface temperature, across the range of climates simulated. The tropical-mean (averaged between +10° and −10° latitudes) tropopause height is shown with a black line, the LCL (850 hPa) is shown with a dotted line, and the pressure at which the absolute value of the average vertical velocity profile is maximum for each climate, computed through a cubic spline fit to the profiles in (a), is shown with white dots.

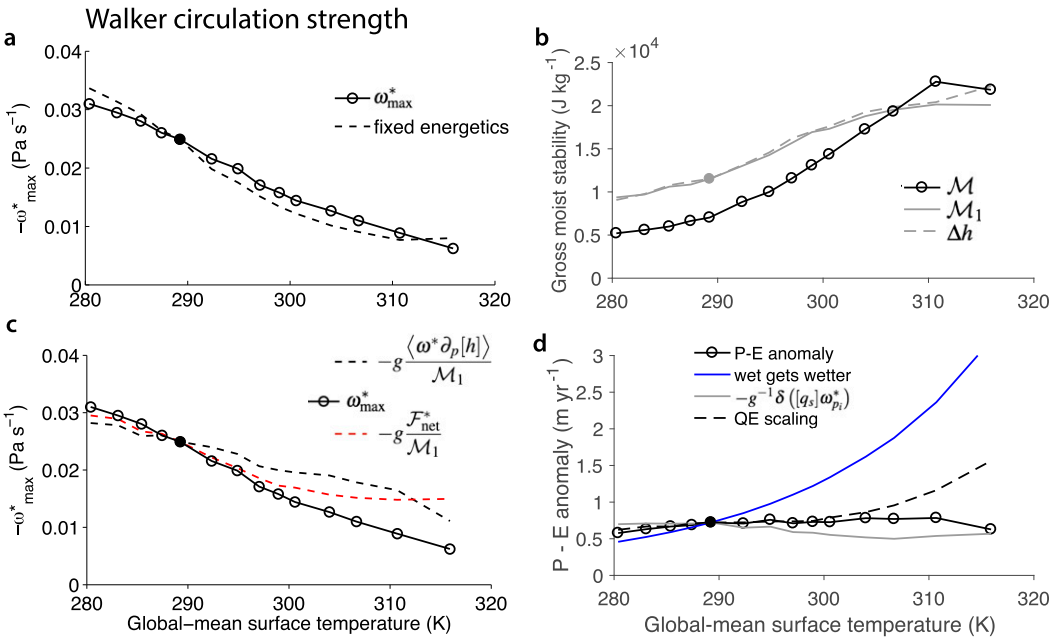

FIG. 4. Walker circulation strength, GMS, and scalings, averaged over the ascent region. (a) Walker circulation strength $-\omega^*_{\max}$ (solid black line) and an estimate of the Walker circulation that would result without changes in column energetics (i.e., a scaling $\propto \mathcal{M}^{-1}$, dashed black line). (b) Walker circulation GMS $\mathcal{M}$ across the range of climates and estimates based on baroclinic mode theory $\mathcal{M}_1$ and on the tropical-mean MSE difference Δh between the tropopause and the LCL [Eq. (15)], with Δh normalized by $\mathcal{M}_1$ in the reference climate (289 K, filled circle). (c) Walker circulation strength and scaling estimates based on $\langle \omega^* \partial_p [h] \rangle$ or $\mathcal{F}^*_{\text{net}}$ and the GMS estimate $\mathcal{M}_1$ [Eq. (14)]. (d) Scalings for zonally anomalous $P - E$ in the ascent region based on the moisture budget scaling [Eq. (17), solid gray line] and the QE moisture budget scaling [Eq. (18), dashed black line]. The purely thermodynamic wet-gets-wetter scaling, based on the increase of surface specific humidity, with no change in circulation, is shown for reference (blue line). All scalings in (a),(c), and (d) are normalized in the reference climate (289 K, filled circle).

balance in the real world, the scaling (10) provides a useful framework for diagnosing the mechanisms behind changes in Walker circulation strength in comprehensive climate models and in observations. It is important to note that $\mathcal{F}^*_{\text{net}}$ is no longer an external forcing when zonal anomalies of shortwave and longwave radiative tendencies depend on the Walker circulation strength through the cloud and water vapor radiative effects.

The GMS, as measured by $\mathcal{M}$, is an empirical quantity that summarizes how much energy large-scale tropical circulations export out of convective regions per unit mass flux, thus characterizing the sensitivity of the Walker circulation to energetic forcing. The GMS concept has also been used to understand changes in the strength of the Hadley circulation (Kang et al. 2009), but GMS differs for different types of circulations, because it depends on the vertical structure of the relevant vertical velocities. Next, we show how baroclinic mode theory can be used to determine the Walker circulation GMS from the zonal-mean climate state.

c. *A first baroclinic mode theory of GMS*

To derive an approximate GMS from its definition (8), we need to factor the vertical velocity out of the vertical integral in the vertical advection term, $\langle \omega^* \partial_p [h] \rangle$. This requires knowledge of the vertical structure of zonally anomalous circulations.

Deep zonally anomalous circulations in the tropics are well described by the first baroclinic mode (Neelin and Zeng 2000) and can thus be expressed through a separation of variables as

$$\omega^*(\mathbf{x}, p) \approx -\Omega_1(p) \nabla \cdot \mathbf{u}_1(\mathbf{x}). \tag{11}$$

Here, $\Omega_1(p)$ contains all information about the vertical structure of vertical velocities and $\nabla \cdot \mathbf{u}_1(\mathbf{x})$ contains information about the horizontal variations of zonally anomalous divergence. In regions of weak temperature gradients (Sobel et al. 2001) and convective quasi equilibrium (Emanuel 2007; Neelin 2007), $\Omega_1(p)$ can be calculated explicitly based on a linearization of temperature anomalies about a tropical-mean temperature profile $T_r(p)$ (averaged between $+10°$ and $-10°$ latitudes):

$$T(\mathbf{x}, p) \approx T_r(p) + A_1(p)T_1(\mathbf{x}). \quad (12)$$

Here, $T_1(\mathbf{x})$ is the zonal temperature anomaly at the LCL and $A_1(p)$ describes the sensitivity of free-tropospheric temperature to perturbations at the LCL based on convective quasi-equilibrium (QE) theory, where saturation MSE is constant above the LCL (Emanuel et al. 1994; Emanuel 2007; Neelin and Zeng 2000). The sensitivities of tropospheric horizontal and vertical winds, $V_1(p)$ and $\Omega_1(p)$, to perturbations at the LCL follow from the application of the momentum equation and continuity equation. This approach was developed by Neelin and Yu (1994) and Yu and Neelin (1997) [see also review by Neelin (2007)].

We compute the temperature mode $A_1(p)$ and wind mode $\Omega_1(p)$ following Levine and Boos (2016), who present a generalization of the QE model found in Neelin and Zeng (2000). The generalization relaxes some of the approximations on the relative importance of temperature, moisture, and geopotential for MSE, such that the $\Omega_1(p)$ modes are relevant over the full range of climates in the idealized GCM simulations (see the derivation in appendix A). We impose a fixed LCL height of 850 hPa, which is consistent with small changes in relative humidity (Schneider et al. 2010). The result is that $A_1(p)$ and $\Omega_1(p)$ are determined uniquely from the tropical-mean temperature profile $T_r(p)$. The QE vertical velocity profiles $\Omega_1(p)$ (Fig. 5b) are similar to the vertical velocity profiles in the ascent region as simulated by the idealized GCM (Fig. 5a). The GCM vertical velocity profiles in Fig. 5a are normalized such that their maximum value is the same as the maximum value of $\Omega_1(p)$. Departures of the vertical velocity profiles from QE are largest near the surface, near the tropopause, and in the warmest climates (Fig. 5c), but overall, QE baroclinic modes capture the vertical velocity structure well in these simulations.

By combining the baroclinic mode decomposition (11) with the GMS definition (8), we obtain an approximate GMS:

$$\mathcal{M}_1 \equiv -g\frac{\langle \Omega_1(p)\partial_p[h]\rangle}{\Omega_1^{\max}} \approx \mathcal{M}. \quad (13)$$

Here, $\Omega_1^{\max}$ is the maximum value of $\Omega_1(p)$. The zonal-mean MSE stratification $\partial_p[h]$ is averaged between +10° and −10° latitudes for consistency with the tropical averages used in calculating $\Omega_1(p)$. The QE GMS $\mathcal{M}_1$ expresses the export of MSE by a typical first baroclinic perturbation, per unit convective mass flux. It increases strongly with warming throughout the range of climates, similar to the empirical GMS $\mathcal{M}$ (Fig. 4b). Differences between $\mathcal{M}$ and $\mathcal{M}_1$ (Fig. 4b) show departures of the vertical velocity profiles from the QE profiles (Fig. 5c). This QE methodology has similarly been used to diagnose an increase in GMS with warming in comprehensive climate models (Chou and Neelin 2004; Chou et al. 2013).

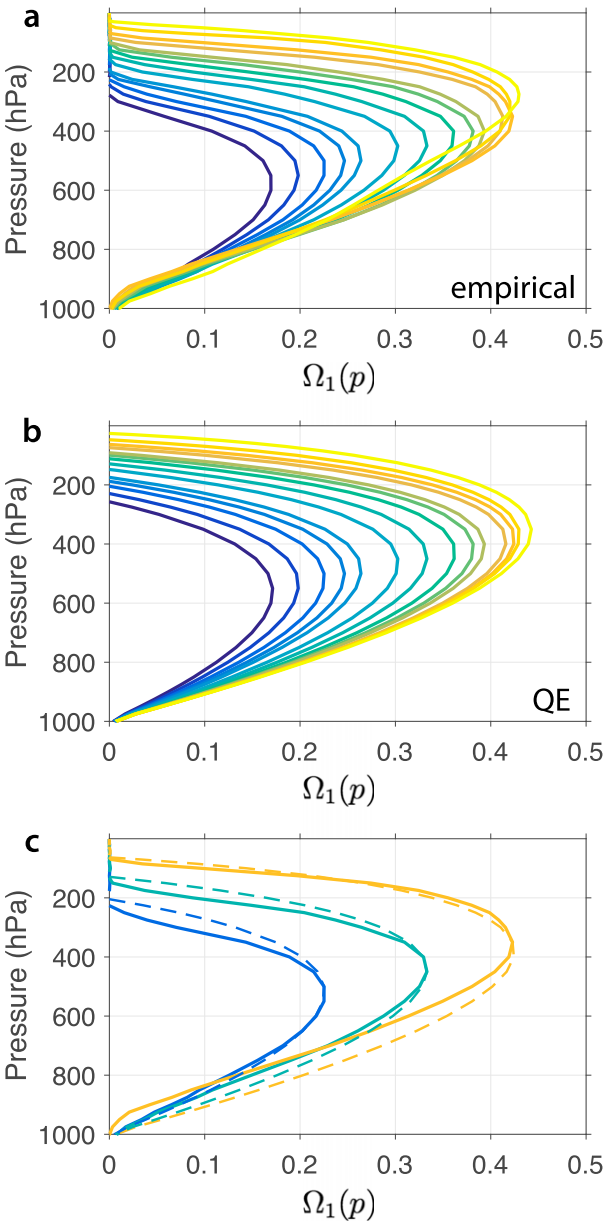

FIG. 5. (a) Nondimensional stationary-eddy vertical velocity profiles, normalized such that the maximum value is the same as the QE $\Omega_1(p)$ profile. (b) Nondimensional QE vertical velocity profile $\Omega_1(p)$. Profiles are shown for 14 mean climate states color coded from coldest (blue) to warmest (yellow). (c) Empirical (solid lines) and QE (dashed lines) vertical velocity profiles for three selected climates, for ease of comparison: α = 0.8, 1.4, and 3.0.

The baroclinic mode GMS $\mathcal{M}_1$ provides an estimate of GMS based solely on the tropical-mean profiles of

temperature and MSE. Specific humidity scales with saturation specific humidity, because relative humidity changes little near the surface (Held and Soden 2000, 2006; Schneider et al. 2010), where atmospheric moisture is concentrated. This means that tropical-mean specific humidity profiles can be determined from tropical-mean temperature profiles and a reference relative humidity. Therefore, the MSE profile is primarily determined by the temperature profile. Furthermore, the tropical-mean profile of temperature and thus MSE can be estimated from simulations of radiative–convective equilibrium (RCE), which are described in appendix B. GMS can thus be thought of as an external parameter in the response of zonally asymmetric tropical circulations to climate change, determined primarily by RCE within a single column.

The Walker circulation strength is determined by the net zonally anomalous energy input to the atmosphere and the approximate GMS based on QE:

$$\omega^*_{\max} \sim -g\frac{\langle \omega^* \partial_p [h] \rangle}{\mathcal{M}_1} \sim -g\frac{\mathcal{F}^*_{\text{net}}}{\mathcal{M}_1}. \tag{14}$$

These scalings both underestimate $\omega^*_{\max}$ by nearly a factor of 2 because of systematic overestimation of $\mathcal{M}$ by $\mathcal{M}_1$, but they do provide an accurate scaling for changes in $\omega^*_{\max}$ in the cooler and moderately warm climates when their values are fixed to $\omega^*_{\max}$ in the reference climate (Fig. 4c). Because the baroclinic mode GMS $\mathcal{M}_1$ underestimates changes in the GMS $\mathcal{M}$, these scalings lead to an underestimate of the total reduction in circulation strength between the coldest and warmest climates.

Levine and Boos (2016) use the same method for computing $\Omega_1(p)$ and combine it with the linear vorticity balance to account for zonally anomalous circulation changes in the subtropics. However, we found this method to be inaccurate in the deep tropics because nonlinearities in the vorticity budget are important. An analysis of the vorticity budget as the aspect ratio (zonal vs meridional elongation) of the ocean heat flux convergence anomaly is varied reveals a near-constant Walker circulation strength despite large changes in the underlying vorticity balance [see sections 6.2 and 6.3 of Wills (2016)]. In equatorially confined Walker circulations, the vertical motion is maintained by transient-eddy vorticity tendencies, while in wider Walker circulations, the vertical motion is partially maintained by a linear vorticity balance. This further suggests that Walker circulations are energetically controlled and that the vorticity equation adjusts to the time-mean circulation by whatever means possible given the background environment. Levine and Boos (2016) find subtropical circulations to be first baroclinic across a wide range of climates, suggesting that the energy export by divergent circulations in the subtropics could also be quantified using the GMS constraint (13). However, the divergent energy export would not be directly related to the net energy input [i.e., Eq. (7) would not hold], because horizontal MSE advection is important in the subtropics.

d. Sensitivity of Walker circulation to Q-flux changes

Based on the scalings (10) and (14), the strength of the Walker circulation should be proportional to the zonally anomalous net energy input $\mathcal{F}^*_{\text{net}}$. Because $\mathcal{F}^*_{\text{net}}$ is determined by the imposed ocean heat flux convergence in our simulations, the Walker circulation strength should linearly increase with the imposed forcing. We test this by running a sensitivity test, varying Q_1 from 10 to $100\,\text{W}\,\text{m}^{-2}$ in $10\,\text{W}\,\text{m}^{-2}$ increments. The resulting zonally anomalous net energy input and Walker circulation strength are shown in Fig. 6. The Walker circulation strength responds sublinearly because there is an increasingly important damping by transient-eddy MSE fluxes as the forcing amplitude is increased. This reduces the energy available for time-mean updrafts (solid vs dashed black line in Fig. 6a). In the simulation with the strongest forcing, there is a reduction in Walker circulation strength of 35% compared to the linear extrapolation from the simulation with the weakest forcing (Fig. 6b). The sublinear change in Walker circulation strength is predicted correctly if $\langle \omega^* \partial_p h \rangle$ is included in the scaling (14) (dashed black line in Fig. 6b). The GMS determines the linear sensitivity of the Walker circulation strength to imposed energy fluxes (slope of lines in Fig. 6b). Departures from linearity are caused by zonally anomalous transient-eddy MSE fluxes, which reduce the Walker circulation strength as the forcing amplitude increases, so that the response becomes more nonlinear.

e. Sensitivity of GMS to tropopause height and lower-tropospheric specific humidity

The GMS is a difficult quantity to calculate from observations because it depends sensitively on the vertical structures of vertical winds and MSE. For this reason, it is useful to make further approximations to the vertical structure. If, for example, the vertical velocity profile were approximated by a uniform profile between the LCL and the tropopause and zero otherwise, the GMS would simplify to

$$\Delta h \equiv [h_{\text{tropopause}}] - [h_{\text{LCL}}]. \tag{15}$$

The motivation for choosing the LCL instead of the surface as the lower boundary of the integral is to

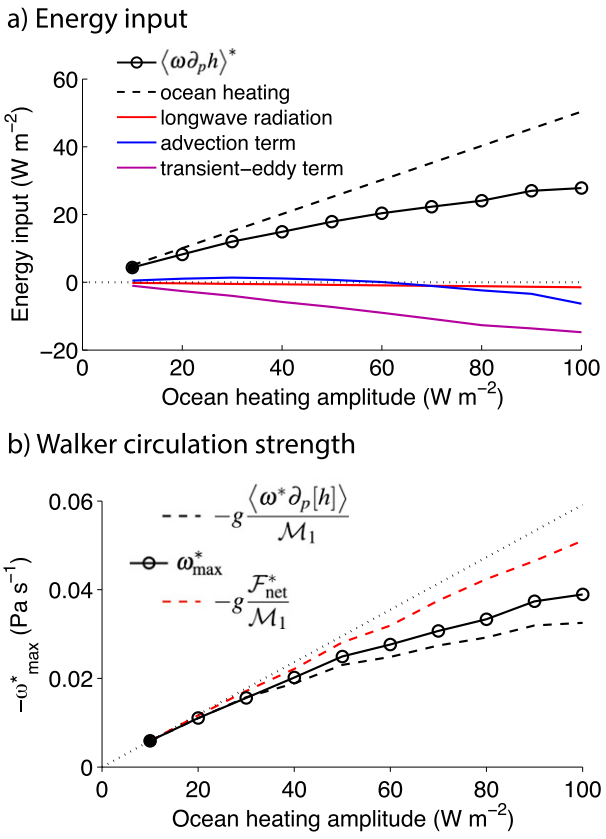

FIG. 6. Zonally anomalous net energy input to the atmosphere and Walker circulation strength as a function of the strength of zonally anomalous ocean forcing Q_1. Averaging is done over the region where the ocean heat flux convergence is greater than 20% of Q_1. (a) As in Fig. 2, but for the sweep of Q_1. It shows a slight departure of $\langle\omega\partial_p h\rangle^*$ from the imposed ocean heat flux convergence because the importance of transient-eddy MSE fluxes increases with forcing strength. (b) As in Fig. 4c, but for the sweep of Q_1. It shows how well the scalings (14) predict changes in Walker circulation strength. The thin dotted line shows the Walker circulation strength that would result from a linear extrapolation from the 10 W m^{-2} forcing (sold circle).

represent the fact that vertical velocities are small in the boundary layer, where MSE is strongly stratified. This MSE difference Δh would be zero if the stratification were moist adiabatic (Emanuel 2007). It is positive primarily as a result of subsaturation of the atmosphere. Averaged over the tropics (between +10° and −10° latitudes), Δh scales similarly to $\mathcal{M}_1$ across the range of climates (Fig. 4b).

We investigate the temperature, geopotential, and moisture contributions to GMS by splitting Δh into its components (Fig. 7):

$$\Delta h = \Delta T + \Delta\Phi + \Delta q. \tag{16}$$

The geopotential term $\Delta\Phi$ is large and positive throughout the range of climates; it increases with the

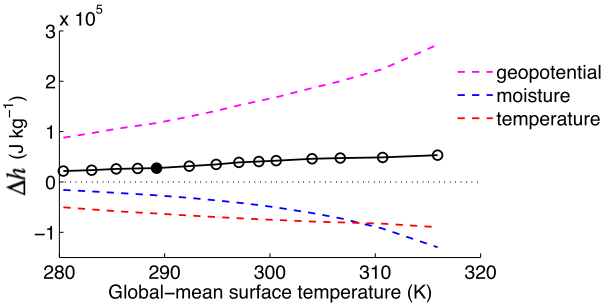

FIG. 7. (a) Decomposition of tropical-mean Δh into components from geopotential $\Delta\Phi$, moisture Δq, and temperature ΔT. The reference-climate value of Δh is indicated with a filled circle. The increase in GMS with warming due to the geopotential term, which increases with tropopause height, overwhelms the decrease in GMS with warming from the temperature and moisture terms, which decrease as the LCL temperature and moisture content increase. Changes in tropopause temperature and moisture content are negligible.

height of the tropopause. Neglecting the small specific humidity near the tropopause, the moisture term $\Delta q \approx -[q_{\rm LCL}]$ shows the Clausius–Clapeyron increase of boundary layer moisture content, which acts to reduce GMS with warming. The dry stratification term ΔT shows the increasing magnitude of the LCL–tropopause temperature difference with warming, which also acts to reduce GMS. This results despite the reduced dry static stability because the tropopause rises. The steady increase in LCL temperature drives the increasing magnitude of ΔT. By contrast, the tropopause temperature varies little as the climate changes in response to increasing atmospheric longwave opacity, as expected from its primary dependence on OLR (Schwarzschild 1906; Schneider 2007). The full GMS, as diagnosed from Δh, is a small residual of these large terms.

Overall, we find that GMS increases with global warming as the troposphere deepens. This increase is only partially offset by the increase of lower-tropospheric specific humidity. Chou and Chen (2010) find this mechanism to operate in intermediate-complexity and comprehensive climate simulations over a limited range of climate change (i.e., doubled CO_2 experiment). Our results suggest that it is relevant over a much wider range of climates. While the fractional changes are largest for Δq, the larger value of $\Delta\Phi$ in the reference climate means that it dominates changes in Δh across the range of climates studied. GMS is thus positive and increases with warming.

4. Sensitivity of Walker circulation $P - E$ anomalies to global warming

The scalings (10) and (14) for the Walker circulation strength can be applied to understand changes in zonally

anomalous $P - E$ over the ascent region, which are small ($<2\%\,\mathrm{K}^{-1}$) in our simulations (Fig. 4d; cf. Wills and Schneider 2016). In this way, we can provide a mechanistic reason for the relatively constant $P - E$ and P anomalies in our simulations and in the similar simulations of Merlis and Schneider (2011). Changes in zonally anomalous $P - E$ have been shown to be governed by changes in zonally anomalous vertical velocities $\omega^*_{p_i}$ in the lower troposphere and changes in zonal-mean surface specific humidity (Wills and Schneider 2016; Wills et al. 2016):

$$P^* - E^* \sim -g^{-1}[q_s]\omega^*_{p_i}. \tag{17}$$

Here, p_i is a lower-tropospheric reference pressure. With $p_i = 800\,\mathrm{hPa}$, this scaling captures the lack of change in zonally anomalous $P - E$ throughout the range of climates (solid line, Fig. 4d).[1] The decrease in circulation strength cancels the increase in surface specific humidity, which would otherwise lead to a strong wet-gets-wetter effect (blue line, Fig. 4d). This moisture budget approximation can be combined with the baroclinic mode circulation strength scaling (14) to relate the $P - E$ anomaly to the zonally anomalous net energy input $\mathcal{F}^*_{\mathrm{net}}$ and the baroclinic mode GMS estimate $\mathcal{M}_1$ (dashed line, Fig. 4d):

$$P^* - E^* \sim [q_s]\frac{\mathcal{F}^*_{\mathrm{net}}}{\mathcal{M}_1}\frac{\Omega_1(800\,\mathrm{hPa})}{\Omega_1^{\max}}. \tag{18}$$

Here, we used the vertical wind mode $\Omega_1(p)$ to convert the scaling (14) for $\omega^*_{\max}$ into a scaling for $\omega^*(p)$ at 800 hPa. This provides an accurate $P - E$ scaling in all but the warmest climates, where $P - E$ is overestimated owing to an overestimation of $\omega^*(p)$. The zonal-mean specific humidity $[q_s]$ and baroclinic mode GMS estimate $\mathcal{M}_1$ both change substantially with warming, but they influence $P - E$ anomalies in opposite ways. The lack of change in $P - E$ anomaly results from the cancellation of changes in these two terms.

5. Discussion

Much of the early work on Walker circulations has focused on the role of tropical SSTs (Bjerknes 1969, 1972). SSTs are more easily measured than the surface and top-of-atmosphere energy fluxes that are used in the theory of this paper. Fortunately, there exists a link between SSTs and evaporation, which is the dominant energetic term that balances ocean heat flux convergence. Merlis and Schneider (2011) show that in similar aquaplanet GCM simulations, east–west differences in evaporation ΔE are dominated by east–west differences in saturation specific humidity q_s, which are a function of east–west differences in SST (ignoring air–sea temperature differences):

$$\Delta E \sim \Delta q_s(\mathrm{SST}). \tag{19}$$

This relation can be inverted to give an expression for the east–west SST difference (ΔSST):

$$\Delta\mathrm{SST} \sim \left(\frac{\partial q_s}{\partial T}\right)^{-1}\Delta E. \tag{20}$$

The result is that the east–west differences in evaporation and SST are linearly related, though with a thermodynamic coefficient that varies strongly with mean temperature through the Clausius–Clapeyron relationship.

The implication of this, given the approximate linearity of the Walker circulation response to energetic forcing (Fig. 6), is that the sensitivity of Walker circulations to SST gradients could depend on mean temperature. However, in our idealized GCM experiments, as the mean climate is warmed, the decreasing thermodynamic coefficient in Eq. (20) is offset by the increase in gross moist stability such that fractional changes in Walker circulation strength are similar to fractional changes in SST gradient across the range of climates (Fig. 8). This is qualitatively consistent with observations and comprehensive climate simulations of the past century, which have shown a concomitant weakening of the Walker circulation and zonal SST gradient in the equatorial Pacific (Tokinaga et al. 2012). Further modeling studies are required to test if this cancellation always occurs in this way, such that SST gradients and Walker circulation strength are approximately linearly related across a wide range of climates.

In the real climate system, the zonally anomalous net energy input will include radiative effects of clouds and water vapor. Knutson and Manabe (1995) show that there is an increase in the clear-sky radiative cooling of the western Pacific with warming, arising primarily from the increase in atmospheric moisture content in this region. This radiative cooling reduces the Walker circulation strength according to our energetic framework. Peters and Bretherton (2005) used an idealized model of the Walker circulation to investigate the role of water vapor and cloud radiative effects in more detail. They also find that clear-sky radiative fluxes dominate

[1] This scaling works well for other choices of p_i in the lower troposphere. We choose 800 hPa to emphasize that this does not need to be the same as the LCL pressure.

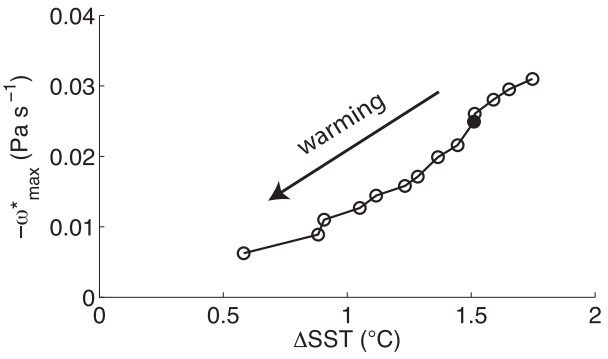

FIG. 8. The decrease in Walker circulation strength (as in Fig. 4a) and east–west temperature difference (ΔSST; as measured by the difference in surface temperature between ascent and descent regions, both defined where $|\mathcal{Q}| > 10$ W m^{-2}) across the range of climates in the idealized GCM. The reference climate (289-K global-mean surface temperature) is indicated with a filled circle.

tropospheric radiative cooling changes and, thus, exert an important influence on the strength of the Walker circulation.

High clouds, which dominate the cloud climatology in the ascending branch of the Walker circulation, do not have a large influence on the zonally anomalous energy input, because of a cancellation between heating from longwave absorption and cooling from shortwave reflection (Ramanathan et al. 1989; Harrison et al. 1990; Hartmann et al. 2001). Therefore, high clouds have only a small influence on the Walker circulation strength (Peters and Bretherton 2005). Low clouds, however, provide a strong column-integrated cooling because their albedo effect dominates over their greenhouse effect (Ockert-Bell and Hartmann 1992; Hartmann et al. 1992). Their column cooling reduces the zonal-mean radiative heating in the tropics. The relative lack of low clouds in the warm pool would thus result in a positive zonally anomalous net energy input, increasing the climatological Walker circulation strength. This agrees with the results of Peters and Bretherton (2005). Any changes in low clouds would have a corresponding influence on the Walker circulation strength (e.g., an increase in low-cloud reflection in the descending branch would increase the strength of the Walker circulation).

6. Conclusions

The relationships (9), (10), and (14) for the Walker circulation strength provide a simple picture of how local energetic constraints can lead to a slowdown of the Walker circulation with global warming. They predict the strength of the Walker circulation associated with zonally anomalous sources and sinks of MSE. Changes in the denominator of these expressions illustrate the anomalous gross moist stability mechanism of Chou and Neelin (2004). Other MSE based mechanisms involve changes in the numerator, such as the upped-ante mechanism (Chou and Neelin 2004; Chou et al. 2009) based on changes in the horizontal advection of MSE. The response to global warming in our simulations is dominated by an increase in GMS due to the increasing depth of the troposphere, which leads to a weakening of the Walker circulation throughout the range of climates (Fig. 4c; cf. Chou and Chen 2010).

The gross moist stability (GMS) provides a measure of how much energy is exported out of deep convective regions per unit convective mass flux. As the mean climate warms, convective outflows transport more energy per unit convective mass flux. The GMS depends on the vertical structure of zonally anomalous tropical circulations, which, for deep circulation, is well described by the first baroclinic mode (Neelin and Zeng 2000). Using convective quasi-equilibrium theory, we have derived an approximation for the GMS that captures its increase with warming. The GMS for the Walker circulation is thus primarily determined by the tropical-mean temperature and MSE profiles, which are close to those determined from radiative–convective equilibrium (RCE). The increase of GMS and decrease of Walker circulation strength with warming are well captured by QE and RCE.

Our analysis reveals that the Walker circulation weakens with warming in our idealized GCM simulations as a result of the increase in tropopause height. The increasing tropopause height leads to an increasing difference in gravitational potential energy between convective inflows and outflows, which dominates smaller changes in LCL temperature and moisture content, leading to an increase in GMS. These dominant influences on GMS and Walker circulation strength are illustrated schematically in Fig. 9. The take-home understanding is that the Walker circulation strength is set locally by the energy available. The GMS determines the sensitivity to this energetic forcing by characterizing the energy exported out of the convective region per unit convective mass flux:

$$\text{Walker circulation strength} = \frac{\text{Total zonally anomalous energy input to the atmospheric column}}{\text{Energy export per unit convective mass flux}}. \quad (21)$$

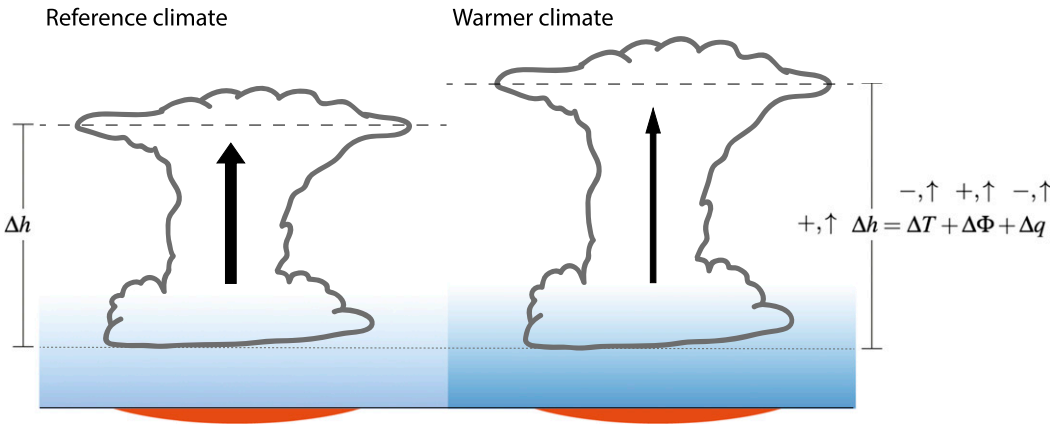

FIG. 9. Schematic of factors that influence the Walker circulation as the climate warms. With fixed ocean heat flux forcing (orange), the Walker circulation decreases in strength (black arrows), predominantly owing to the increased energetic requirements of reaching a higher tropopause height (dashed line), where the deepest convective parcels reach their level of neutral buoyancy. The enhanced boundary layer moisture content (blue shading) is the dominant reason for the higher level of neutral buoyancy (through its influence on reducing the moist adiabatic lapse rate), but it also acts to reduce the energetic requirements of time-mean updrafts, moderating the tropopause height influence. These influences are characterized by the MSE difference Δh between the LCL (dotted line) and the tropopause (dashed line). The MSE difference Δh increases with warming because the increase in tropopause depth $\Delta\Phi$ dominates smaller changes in bulk moisture and temperature stratification, Δq and ΔT. Increases in magnitude with warming are indicated by ↑. Contributions that are positive (negative) are indicated by plus (minus) signs.

Acknowledgments. The idealized GCM simulations for this study were performed on ETH Zürich's EULER computing cluster. We thank Simona Bordoni, Jess Adkins, Andy Thompson, Michael Byrne, and Chris Bretherton for useful comments and discussion during the development of this manuscript.

APPENDIX A

Derivation of Vertical Velocity Mode

The derivation of the vertical wind modes $\Omega_1(p)$ follows Levine and Boos (2016).

The basis for an understanding of the vertical structure of perturbations to the tropical atmosphere is that variations in saturation moist static energy (MSE) are invariant with height above the LCL (Arakawa and Schubert 1974; Emanuel et al. 1994; Emanuel 2007), a state called convective quasi equilibrium (QE). Temperature variations at a pressure p can be related to the saturation MSE $h_{\rm sat}$ by differentiating the expression for saturation MSE with respect to temperature,

$$\frac{1}{c_p}\frac{dh_{\rm sat}}{dT}\bigg|_p = 1 + z_T + q_T, \tag{A1}$$

where

$$q_T = \frac{L}{c_p}\frac{dq_{\rm sat}}{dT}\bigg|_p = \frac{L^2(q_{\rm sat})_r}{c_p r_v T_r^2}\left(1 + \frac{r_v}{r_d}q_{\rm sat} - q_{\rm sat}\right)_r \tag{A2}$$

and

$$z_T = \frac{g}{c_p}\frac{dz}{dT}\bigg|_p = -\frac{r_d}{c_p}\log\frac{p}{p_s}. \tag{A3}$$

Here $q_{\rm sat}$ is the saturation specific humidity, L is the specific latent heat of vaporization, r_v and r_d are the specific gas constants of water vapor and dry air, respectively, and c_p is the specific heat capacity at constant pressure. Note that temperature and saturation specific humidity are defined in their native units throughout the appendix (as opposed to the main text, where they are in units of joules per kilogram). Hydrostatic balance was used to express the sensitivity of geopotential height to temperature as a function of pressure. These expressions depend on the tropical-mean temperature T_r and saturation specific humidity $(q_{\rm sat})_r$, where $(\cdot)_r$ denotes a tropical average (averaged between +10° and −10° latitudes) at constant p.

Similarly, LCL temperature variations can be related to LCL saturation MSE variations,

$$\frac{1}{c_p}\left(\frac{dh_{\rm sat}}{dT}\right)_b = 1 + (z_T)_b + (q_T)_b, \tag{A4}$$

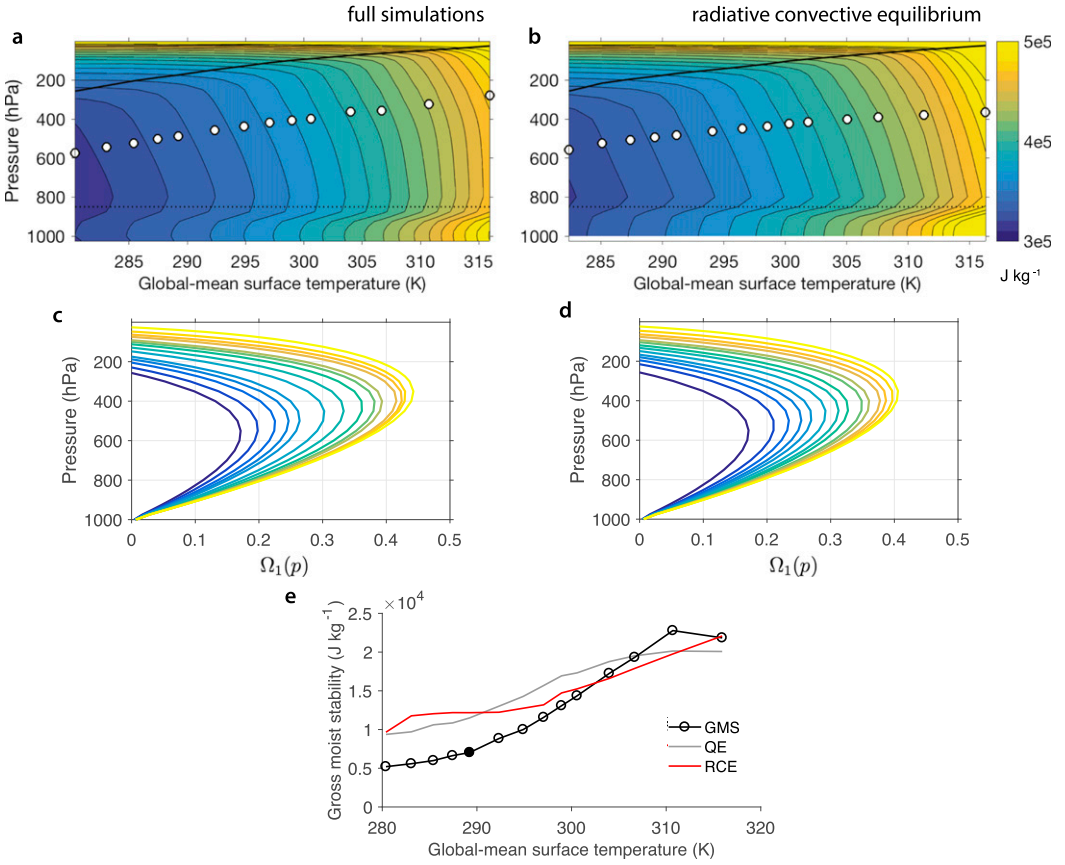

FIG. B1. Vertical profile of tropical-mean (averaged between +10° and −10° latitudes) MSE in (a) the full simulations and (b) the RCE simulations, as a function of global-mean surface temperature, across the range of climates simulated. The tropical-mean tropopause height is shown with a black line, the LCL (850 hPa) is shown with a dotted line, and the pressure at which $\Omega_1(p)$ is maximum for each climate, computed through a cubic spline fit to the profiles in (c) and (d), is shown with white dots. Nondimensional QE vertical velocity profile $\Omega_1(p)$ for (c) the full simulations and (d) the RCE simulations. Profiles are shown for 14 mean climate states color coded from coldest (blue) to warmest (yellow). (e) Walker circulation GMS $\mathcal{M}$ (line with circles) across the range of climates and estimates based on baroclinic mode theory $\mathcal{M}_1$ (solid line) and from $\mathcal{M}_1$ computed with the temperature and MSE profiles from RCE (red line).

where the subscript b denotes LCL values. This allows us to define a temperature mode, which relates variations in LCL temperature to variations in temperature in the free troposphere,

$$A_1(p) \equiv \left.\frac{dT}{dT_b}\right|_p = \left(\frac{dh_{\rm sat}}{dT}\right)_b \left(\left.\frac{dh_{\rm sat}}{dT}\right|_p\right)^{-1} = \frac{1+(z_T)_b+(q_T)_b}{1+z_T+q_T}. \quad \text{(A5)}$$

The QE circulation model introduced by Neelin and Zeng (2000) makes further simplifications of this expression as detailed in Levine and Boos (2016). We use the full expression [Eq. (A5)] in order to best capture changes in the vertical structure of tropical perturbations across a wide range of climates.

The sensitivity of free-tropospheric temperature to changes in low-level temperature is nearly invariant in the tropics, as temperature cannot be significantly different from its tropical-mean profile (Charney 1963; Sobel et al. 2001). This state of weak temperature gradients in the tropics allows us to linearize temperature,

$$T(\mathbf{x}, p, t) \approx T_r(p) + A_1(p) \cdot T_1(\mathbf{x}, t), \quad \text{(A6)}$$

where T_r defines the tropical-mean temperature profile and T_1 is the local temperature anomaly at the LCL.

On Earth, tropical circulations show a dominant baroclinic structure (e.g., Trenberth et al. 2000), consistent with circulations being thermally driven and divergent to first order. In this scenario, it is useful to decompose horizontal winds into barotropic and baroclinic components, $\mathbf{u}(\mathbf{x}, p, t) = \mathbf{u}_r(p) + V_1(p) \cdot \mathbf{u}_1(\mathbf{x}, t)$.

By plugging modal decompositions for temperature and horizontal winds into the momentum equation in a hydrostatic atmosphere, we obtain an expression for $V_1(p)$, the vertical structure of the baroclinic wind:

$$V_1(p) = A_1^+ - \frac{1}{p_t - p_s}\int_{p_s}^{p_t} A_1^+ \, dp, \tag{A7}$$

where

$$A_1^+ = \int_{p_s}^{p} A_1 \, dp \tag{A8}$$

and p_t is the tropopause pressure.

Finally, we solve for the vertical structure of vertical velocity in baroclinic perturbations by using continuity, obtaining

$$\Omega_1(p) = \frac{1}{p_s}\int_{p_s}^{p} V_1 \, dp. \tag{A9}$$

The result is that $\Omega_1(p)$ is determined from the temperature mode [Eq. (A5)] through use of the relations (A7)–(A9). Because of multiple tropospheric averages, the vertical wind mode is quite sensitive to changes in the tropopause height.

APPENDIX B

Radiative–Convective Equilibrium Simulations

The zonal-mean GMS estimate $\mathcal{M}_1$ is computed entirely from the tropical-mean temperature and MSE profiles. GMS can thus be thought of as an external parameter in the response of circulations to climate change, to the extent that the temperature and MSE profiles are consistent with radiative–convective equilibrium (RCE). We test this with a radiative–convective model of the atmosphere, which is constructed from the idealized moist GCM by disabling all lateral fluxes in the atmosphere. The atmosphere adjusts directly to local radiative and surface enthalpy fluxes, with convection and boundary layer turbulent fluxes acting to homogenize MSE and specific humidity in the air column. Parameterizations for surface latent and sensible heat fluxes, boundary layer fluxes, and vertical diffusive fluxes require a horizontal wind profile to be prescribed; here, we apply a uniform wind of $2\,\mathrm{m\,s^{-1}}$. This RCE model is identical to that described in O'Gorman and Schneider (2008) and Schneider and O'Gorman (2008), except for the prescribed value of horizontal wind. The zonal-mean MSE profiles in the RCE simulations (Fig. B1) look similar to those in the full simulations, despite an offset in global-mean surface temperature and corresponding offset in MSE at all levels. The QE baroclinic mode profiles $\Omega_1(p)$ in the RCE simulations are also comparable to those in the full simulations. The GMS computed from the RCE simulations shows a similar change across the range of climates to the full GCM, though with some differences in intermediate climates. This suggests that GMS changes can be estimated from a single-column model.

REFERENCES

Arakawa, A., and W. H. Schubert, 1974: Interaction of a cumulus cloud ensemble with the large-scale environment, Part I. *J. Atmos. Sci.*, **31**, 674–701, doi:10.1175/1520-0469(1974)031<0674:IOACCE>2.0.CO;2.

Betts, A. K., 1998: Climate-convection feedbacks: Some further issues. *Climatic Change*, **39**, 35–38, doi:10.1023/A:1005323805826.

Bjerknes, J., 1969: Atmospheric teleconnections from the equatorial Pacific. *Mon. Wea. Rev.*, **97**, 163–172, doi:10.1175/1520-0493(1969)097<0163:ATFTEP>2.3.CO;2.

——, 1972: Large-scale atmospheric response to the 1964–65 Pacific equatorial warming. *J. Phys. Oceanogr.*, **2**, 212–217, doi:10.1175/1520-0485(1972)002<0212:LSARTT>2.0.CO;2.

Bordoni, S., and T. Schneider, 2008: Monsoons as eddy-mediated regime transitions of the tropical overturning circulation. *Nat. Geosci.*, **1**, 515–519, doi:10.1038/ngeo248.

Chadwick, R., I. Boutle, and G. Martin, 2013: Spatial patterns of precipitation change in CMIP5: Why the rich do not get richer in the tropics. *J. Climate*, **26**, 3803–3822, doi:10.1175/JCLI-D-12-00543.1.

Charney, J. G., 1963: A note on large-scale motions in the tropics. *J. Atmos. Sci.*, **20**, 607–609, doi:10.1175/1520-0469(1963)020<0607:ANOLSM>2.0.CO;2.

Chou, C., and J. D. Neelin, 2004: Mechanisms of global warming impacts on regional tropical precipitation. *J. Climate*, **17**, 2688–2701, doi:10.1175/1520-0442(2004)017<2688:MOGWIO>2.0.CO;2.

——, and C.-A. Chen, 2010: Depth of convection and the weakening of tropical circulation in global warming. *J. Climate*, **23**, 3019–3030, doi:10.1175/2010JCLI3383.1.

——, J. D. Neelin, C.-A. Chen, and J.-Y. Tu, 2009: Evaluating the "rich-get-richer" mechanism in tropical precipitation change under global warming. *J. Climate*, **22**, 1982–2005, doi:10.1175/2008JCLI2471.1.

——, T.-C. Wu, and P.-H. Tan, 2013: Changes in gross moist stability in the tropics under global warming. *Climate Dyn.*, **41**, 2481–2496, doi:10.1007/s00382-013-1703-2.

Emanuel, K., 2007: Quasi-equilibrium dynamics of the tropical atmosphere. *The Global Circulation of the Atmosphere*, T. Schneider and A. H. Sobel, Eds., Princeton University Press, 186–218.

——, J. David Neelin, and C. S. Bretherton, 1994: On large-scale circulations in convecting atmospheres. *Quart. J. Roy. Meteor. Soc.*, **120**, 1111–1143, doi:10.1002/qj.49712051902.

Frierson, D. M., 2007: The dynamics of idealized convection schemes and their effect on the zonally averaged tropical circulation. *J. Atmos. Sci.*, **64**, 1959–1976, doi:10.1175/JAS3935.1.

——, I. M. Held, and P. Zurita-Gotor, 2006: A gray-radiation aquaplanet moist GCM. Part I: Static stability and eddy scale. *J. Atmos. Sci.*, **63**, 2548–2566, doi:10.1175/JAS3753.1.

Harrison, E., P. Minnis, B. Barkstrom, V. Ramanathan, R. Cess, and G. Gibson, 1990: Seasonal variation of cloud radiative forcing derived from the Earth Radiation Budget Experiment. *J. Geophys. Res.*, **95**, 18 687–18 703, doi:10.1029/JD095iD11p18687.

Hartmann, D. L., M. E. Ockert-Bell, and M. L. Michelsen, 1992: The effect of cloud type on Earth's energy balance: Global analysis. *J. Climate*, **5**, 1281–1304, doi:10.1175/1520-0442(1992)005<1281:TEOCTO>2.0.CO;2.

——, L. A. Moy, and Q. Fu, 2001: Tropical convection and the energy balance at the top of the atmosphere. *J. Climate*, **14**, 4495–4511, doi:10.1175/1520-0442(2001)014<4495:TCATEB>2.0.CO;2.

Held, I. M., and A. Y. Hou, 1980: Nonlinear axially symmetric circulations in a nearly inviscid atmosphere. *J. Atmos. Sci.*, **37**, 515–533, doi:10.1175/1520-0469(1980)037<0515:NASCIA>2.0.CO;2.

——, and B. J. Soden, 2000: Water vapor feedback and global warming. *Annu. Rev. Energy Environ.*, **25**, 441–475, doi:10.1146/annurev.energy.25.1.441.

——, and ——, 2006: Robust responses of the hydrological cycle to global warming. *J. Climate*, **19**, 5686–5699, doi:10.1175/JCLI3990.1.

Huang, P., S.-P. Xie, K. Hu, G. Huang, and R. Huang, 2013: Patterns of the seasonal response of tropical rainfall to global warming. *Nat. Geosci.*, **6**, 357–361, doi:10.1038/ngeo1792.

Kang, S. M., D. M. Frierson, and I. M. Held, 2009: The tropical response to extratropical thermal forcing in an idealized GCM: The importance of radiative feedbacks and convective parameterization. *J. Atmos. Sci.*, **66**, 2812–2827, doi:10.1175/2009JAS2924.1.

Knutson, T. R., and S. Manabe, 1995: Time-mean response over the tropical Pacific to increased CO_2 in a coupled ocean-atmosphere model. *J. Climate*, **8**, 2181–2199, doi:10.1175/1520-0442(1995)008<2181:TMROTT>2.0.CO;2.

Levine, X. J., and T. Schneider, 2011: Response of the Hadley circulation to climate change in an aquaplanet GCM coupled to a simple representation of ocean heat transport. *J. Atmos. Sci.*, **68**, 769–783, doi:10.1175/2010JAS3553.1.

——, and W. R. Boos, 2016: A mechanism for the response of the zonally asymmetric subtropical hydrologic cycle to global warming. *J. Climate*, **29**, 7851–7867, doi:10.1175/JCLI-D-15-0826.1.

Merlis, T. M., and T. Schneider, 2010: Atmospheric dynamics of earth-like tidally locked aquaplanets. *J. Adv. Model. Earth Syst.*, **2** (13), doi:10.3894/JAMES.2010.2.13.

——, and ——, 2011: Changes in zonal surface temperature gradients and Walker circulations in a wide range of climates. *J. Climate*, **24**, 4757–4768, doi:10.1175/2011JCLI4042.1.

Neelin, J. D., 2007: Moist dynamics of tropical convection zones in monsoons, teleconnections, and global warming. *The Global Circulation of the Atmosphere*, T. Schneider and A. H. Sobel, Eds., Princeton University Press, 267–301.

——, and I. M. Held, 1987: Modeling tropical convergence based on the moist static energy budget. *Mon. Wea. Rev.*, **115**, 3–12, doi:10.1175/1520-0493(1987)115<0003:MTCBOT>2.0.CO;2.

——, and J.-Y. Yu, 1994: Modes of tropical variability under convective adjustment and the Madden–Julian oscillation. Part I: Analytical theory. *J. Atmos. Sci.*, **51**, 1876–1894, doi:10.1175/1520-0469(1994)051<1876:MOTVUC>2.0.CO;2.

——, and N. Zeng, 2000: A quasi-equilibrium tropical circulation model—Formulation. *J. Atmos. Sci.*, **57**, 1741–1766, doi:10.1175/1520-0469(2000)057<1741:AQETCM>2.0.CO;2.

Ockert-Bell, M. E., and D. L. Hartmann, 1992: The effect of cloud type on Earth's energy balance: Results for selected regions. *J. Climate*, **5**, 1157–1171, doi:10.1175/1520-0442(1992)005<1157:TEOCTO>2.0.CO;2.

O'Gorman, P. A., and T. Schneider, 2008: The hydrological cycle over a wide range of climates simulated with an idealized GCM. *J. Climate*, **21**, 3815–3832, doi:10.1175/2007JCLI2065.1.

Peters, M. E., and C. S. Bretherton, 2005: A simplified model of the Walker circulation with an interactive ocean mixed layer and cloud-radiative feedbacks. *J. Climate*, **18**, 4216–4234, doi:10.1175/JCLI3534.1.

Philander, S. G., 1990: *El Niño, La Niña, and the Southern Oscillation*. International Geophysics Series, Vol. 46, Academic Press, 293 pp.

Ramanathan, V., R. D. Cess, E. F. Harrison, P. Minnis, B. R. Barkstrom, E. Ahmad, and D. Hartmann, 1989: Cloud-radiative forcing and climate: Results from the Earth Radiation Budget Experiment. *Science*, **243**, 57–63, doi:10.1126/science.243.4887.57.

Schneider, T., 2006: The general circulation of the atmosphere. *Annu. Rev. Earth Planet. Sci.*, **34**, 655–688, doi:10.1146/annurev.earth.34.031405.125144.

——, 2007: The thermal stratification of the extratropical troposphere. *The Global Circulation of the Atmosphere*, T. Schneider and A. H. Sobel, Eds., Princeton University Press, 267–301.

——, and P. A. O'Gorman, 2008: Moist convection and the thermal stratification of the extratropical troposphere. *J. Atmos. Sci.*, **65**, 3571–3583, doi:10.1175/2008JAS2652.1.

——, ——, and X. J. Levine, 2010: Water vapor and the dynamics of climate changes. *Rev. Geophys.*, **48**, doi:10.1029/2009RG000302.

Schwarzschild, K., 1906: Über das gleichgewicht der sonnenatmosphäre. *Nachr. Ges. Wiss. Goettingen, Math.-Phys. Kl.*, **1906**, 41–53.

Seager, R., Y. Kushnir, C. Herweijer, N. Naik, and J. Velez, 2005: Modeling of tropical forcing of persistent droughts and pluvials over western North America: 1856–2000. *J. Climate*, **18**, 4065–4088, doi:10.1175/JCLI3522.1.

——, N. Naik, and G. A. Vecchi, 2010: Thermodynamic and dynamic mechanisms for large-scale changes in the hydrological cycle in response to global warming. *J. Climate*, **23**, 4651–4668, doi:10.1175/2010JCLI3655.1.

Sobel, A. H., J. Nilsson, and L. M. Polvani, 2001: The weak temperature gradient approximation and balanced tropical moisture waves. *J. Atmos. Sci.*, **58**, 3650–3665, doi:10.1175/1520-0469(2001)058<3650:TWTGAA>2.0.CO;2.

Tokinaga, H., S.-P. Xie, C. Deser, Y. Kosaka, and Y. M. Okumura, 2012: Slowdown of the Walker circulation driven by tropical Indo-Pacific warming. *Nature*, **491**, 439–443, doi:10.1038/nature11576.

Trenberth, K. E., D. P. Stepaniak, and J. M. Caron, 2000: The global monsoon as seen through the divergent atmospheric circulation. *J. Climate*, **13**, 3969–3993, doi:10.1175/1520-0442(2000)013<3969:TGMAST>2.0.CO;2.

Vecchi, G. A., and B. J. Soden, 2007: Global warming and the weakening of the tropical circulation. *J. Climate*, **20**, 4316–4340, doi:10.1175/JCLI4258.1.

——, ——, A. T. Wittenberg, I. M. Held, A. Leetmaa, and M. J. Harrison, 2006: Weakening of tropical Pacific atmospheric circulation due to anthropogenic forcing. *Nature*, **441**, 73–76, doi:10.1038/nature04744.

Walker, C. C., and T. Schneider, 2006: Eddy influences on Hadley circulations: Simulations with an idealized GCM. *J. Atmos. Sci.*, **63**, 3333–3350, doi:10.1175/JAS3821.1.

Wills, R. C., 2016: Stationary eddies and zonal variations of the global hydrological cycle in a changing climate. Ph.D. dissertation, California Institute of Technology, 177 pp. [Available online at http://thesis.library.caltech.edu/9536/.]

——, and T. Schneider, 2016: How stationary eddies shape changes in the hydrological cycle: Zonally asymmetric experiments in an idealized GCM. *J. Climate*, **29**, 3161–3179, doi:10.1175/JCLI-D-15-0781.1.

——, M. P. Byrne, and T. Schneider, 2016: Thermodynamic and dynamic controls on changes in the zonally anomalous hydrological cycle. *Geophys. Res. Lett.*, **43**, 4640–4649, doi:10.1002/2016GL068418.

Xie, S.-P., C. Deser, G. A. Vecchi, J. Ma, H. Teng, and A. T. Wittenberg, 2010: Global warming pattern formation: Sea surface temperature and rainfall. *J. Climate*, **23**, 966–986, doi:10.1175/2009JCLI3329.1.

Yu, J.-Y., and J. D. Neelin, 1997: Analytic approximations for moist convectively adjusted regions. *J. Atmos. Sci.*, **54**, 1054–1063, doi:10.1175/1520-0469(1997)054<1054:AAFMCA>2.0.CO;2.